Available online at www.sciencedirect.com
ScienceDirect
Journal of Molecular Graphics and Modelling 26 (2007) 282–289
Journal of Molecular Graphics and Modelling
www.elsevier.com/locate/JMGM

Differences in electrostatic potential around DNA fragments containing adenine and 8-oxo-adenine An analysis based on regular cylindrical projection

Maciej Harańczyk [a,b], John H. Miller [c], Maciej Gutowski [a,b,d,*]

[a] Chemical Sciences Division, Pacific Northwest National Laboratory, Richland, WA 99352, USA
[b] Department of Chemistry, University of Gdańsk, Sobieskiego 18, 80-952 Gdańsk, Poland
[c] School of Electrical Engineering and Computer Science, Washington State University Tri-Cities, 2710 University Drive, Richland, WA 99352-1671, USA
[d] Chemistry-School of Engineering and Physical Sciences, Heriot-Watt University, Edinburgh EH14 4AS, UK

Received 6 October 2006; received in revised form 8 December 2006; accepted 8 December 2006
Available online 15 December 2006

Abstract

Changes of electrostatic potential (EP) around the DNA molecule resulting from chemical modifications of nucleotides may play a role in enzymatic recognition of damaged sites. Effects of chemical modifications of nucleotides on the structure of DNA have been characterized through large scale density functional theory computations. Quantum mechanical structural optimizations of DNA fragments with three pairs of nucleotides and accompanying counteractions were performed with a B3LYP exchange–correlation functional and 6-31G(d,p) basis sets. The ''intact'' DNA fragment contained adenine in the middle layer, while the ''damaged'' fragment had the adenine replaced with 8-oxo-adenine. The electrostatic potential around these DNA fragments was projected on a cylindrical surface around the double helix. The two-dimensional maps of EP of the intact and damaged DNA fragments were analyzed to identify these modifications of EP that result from the occurrence of 8-oxo-adenine (8oA). It was found that distortions of a phosphate group neighboring 8oA and displacements of the accompanying countercation are clearly reflected in the EP maps.

Keywords: Oxidative DNA damage; 8-Oxo-adenine; Electrostatic potential

1. Introduction

DNA in living cells is continuously exposed to a number of environmental agents, which include UV light and ionizing radiation as well as various chemical species. In many cases, the mechanism of action of these agents involves generation of free radicals that attack DNA and produce a variety of lesions, including sugar and base modifications, strand breaks and DNA–protein cross-links [1]. Some active oxygen radicals (e.g., O_2^-, $^\bullet$OH) are generated endogenously during cellular aerobic metabolism, and the damage they cause may be an important factor in aging and age-dependent diseases, including cancer [2–5]. In other cases, oxygen radicals associated with other substances, known under general name of reactive oxygen species, may be introduced exogenously to the living cells, e.g., with tobacco smoke. They have been recognized as a major etiological factor for cancers of the upper aerodigestive tract [6].

Typically, oxidation of the genomes of aerobic organisms starts from hydroxyl radicals, which add to double bonds of heterocyclic DNA bases and abstract H atom from the methyl group of thymine or each of the five carbon atoms of 2′-deoxyribose [7]. Further reactions of base and sugar radicals generate a variety of modified bases and sugars, base-free sites (abasic sites) and strand breaks. It is beyond the scope of this article to describe the mechanism of oxidative damage to DNA as there are extensive review articles in the literature on this broad subject [8].

* Corresponding author at: Chemistry-School of Engineering and Physical Sciences, Heriot-Watt University, Edinburgh EH14 4AS, UK.
Tel.: +44 131 451 3083; fax: +44 131 451 3180.
E-mail addresses: maharan@chem.univ.gda.pl (M. Harańczyk), jhmiller@tricity.wsu.edu (J.H. Miller), m.gutowski@hw.ac.uk (M. Gutowski).

1093-3263/$ – see front matter © 2007 Elsevier Inc. All rights reserved.
doi:10.1016/j.jmgm.2006.12.005

The most common and representative DNA lesions involve hydroxyl radical attack to pyrimidine and purine bases. The hydroxyl radical additions to C5 and C6 positions of thymine and cytosine, lead to thymine glycol and cytosine glycol, respectively. The corresponding reactions of purine bases involve additions to C8 carbon atom leading to the formation of 8-oxo-purines (after reduction in the second step) or formamidopyrimidine (after oxidation in the second step). The most representative example of an 8-oxo-purine lesion is 8-oxo-guanine (8oG; Fig. 1) that has been extensively studied in the literature. 8oG is seriously genotoxic [9] because the replicative DNA polymerases misread 8oG residues and insert adenine instead of cytosine opposite to the oxidized base. Both bases in the resulting A-8oG mispair are mutagenic lesions, and both undergo base-specific replacements to restore the original C–G pair [10]. Doing so represents a formidable challenge to the DNA repair machinery, because adenine makes up roughly 25% of the bases in most genomes. The 8-oxo-adenine (8oA; Fig. 1) is another example of an 8-oxo-purine lesion but it has not been studied in great detail. However, previous studies show that 8oA and 8oG occur at similar frequencies in mammalian DNA [11,12], and that 8oA is as mutagenic as 8oG [13]. 8oA leads to the A → G transitions and A → C transversions [14].

Oxidative damage to DNA is handled by cellular repair systems and in the majority of cases is successfully repaired [15]. Nature has developed very efficient pathways for repairing sites containing lesions. DNA base damage is thought to be repaired mainly by base-excision repair [16]. The enzymatic DNA damage detection and repair is a complex multi-step process. Base excision repair is initiated by a DNA glycosylase, which recognizes and removes the modified nucleotide by cleavage of the glycosylic bond between the damaged base and deoxyribose. Many glycosylases incise the damaged base by flipping the modified nucleotide out of the helix and into the active site pocket for glycosylic bond cleavage and base release [17–19]. The glycosylase leaves an apurinic/apyrimidinic (AP) site in the DNA, which is processed by AP endonuclease or by the AP lyase activity of the glycosylase.

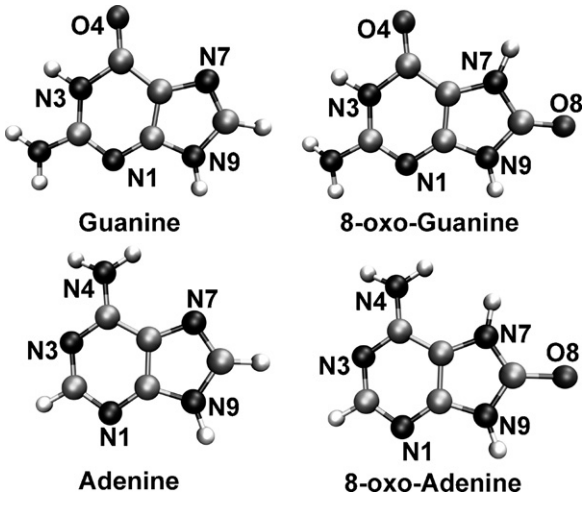

Fig. 1. Purine nucleic acid bases with their 8-oxo-counterparts and atom numbering used in this study.

Despite the fact that damage detection and repair is a complicated process in practice, the idea of damage detection is fairly simple: the enzyme has to locate the damage based on features that make those sites different from intact fragments of DNA. The DNA–enzyme interaction is determined by interactions typical in chemistry: hydrogen bonds, electrostatic interactions and dispersion forces. The two first have the same origin and result from the interaction of effective atomic charges of molecule A with the polarizable charge distribution of molecule B. The dispersion interaction, on the other hand, can be associated with the interaction of instantaneous multipoles of A and B. In the recent work, we analyzed electrostatic potential around an intact DNA fragment and around the same fragment but with guanine being replaced with 8oG [20,21]. Our goal was to identify differences in the electrostatic potential that might be relevant for enzymatic recognition of 8oG.

The electrostatic potential (EP) around DNA is nonuniform because the molecule possesses many polar groups specifically arranged in space. The analysis of electrostatic potential in three dimensions might be a very complex task. However, most of the important interactions take place near the surface of DNA. Hence, we focused our analysis on the values of the electrostatic potential at the ''molecular surface'' [20,21]. For the purpose of our study, we developed and implemented a cylindrical projection of EP, in which the values of the electrostatic potential at the complicated molecular surface of DNA are projected onto the walls of a cylinder, which is built around an approximate DNA axis. The resulting two-dimensional (2D) electrostatic maps were then analyzed for the 5′-TGT-3′ intact fragment of DNA (a fragment containing three nucleic base pairs; the complementary strand is 5′-ACA-3′) and the corresponding fragment containing 8oG in the place of G. The main new features in the EP map resulting from the replacement of G with 8oG were reorganizations of the countercations and phosphate groups. Other new features on the EP map originated from a hydrogen atom at the N7 position and an oxygen atom at the C8 position.

In the current study, we analyze electrostatic potential around the 5′-AAC-3′ DNA trimer and around an analogous trimer with the central A replaced with 8oA. Our algorithm of cylindrical projection of the EP has been greatly improved and extended since the previous report. The major new features are: (1) introduction of solvent-accessible surfaces instead of van der Waals surfaces, (2) usage of electrostatic potential calculated directly from electron density and (3) usage of a reliable molecular axis derived from the tensor of inertia. These new features will be discussed in this report. We have demonstrated that the replacement of A with 8oA leads to a significant reorganization of countercations and phosphate groups. Similarly to the 8oG lesion, these units move along the axis of the DNA fragment away from the C8═O group.

2. Methods

2.1. Molecular structure and introduction of DNA lesions

To obtain the structure of intact and damaged DNA fragments, we use the same approach as described before [20–22]. From a starting molecule, the 5′-GGGAACAACTAG-3′ DNA dodecamer described by Arnott et al. [23], we cut a 5′-AAC-3′ fragment (a trimer) containing three nucleic base pairs (Supplementary data, Fig. S-1). To limit the size of the system, the phosphate groups were removed from the 5′ and 3′ ends, and the strands were saturated with OH groups. The sodium countercations were placed at each of four phosphate groups at the position as they are is in the gas-phase optimized NaH_2PO_4.

The resulting structure was a starting point for density functional theory (DFT) optimizations using a B3LYP exchange–correlation functional [24–26]. In order to suppress computational artifacts resulting from: (i) truncation of the double strand of DNA and (ii) failure to include intermolecular dispersion interaction at the B3LYP level of theory [27], we introduced additional constraints on the trimer. The atoms of the top and bottom nucleic acid base pairs were fixed in space during the optimization [20–22]. This approach guarantees that the failure to include the π–π stacking interaction does not lead to unphysical geometries of the trimer.

The 6-31G(d,p) basis set was used for all geometrically optimized atoms and 6-31G basis set [28] for the geometrically fixed atoms. In the next step, we introduced a lesion. The adenine of the middle layer of the intact 5-AAC-3′ trimer was replaced with 8oA by changing H at the position 8 into oxygen and adding a hydrogen atom to N7. The initial interatomic distances and angles for 8oA in the DNA fragment were the same as those resulting from the B3LYP/6-31G(d,p) optimization for the isolated 8oA. The resulting DNA trimer with 8oA was optimized at the B3LYP level with the same mixed 6-31G/6-31G(d,p) basis set, and again the top and bottom pairs of nucleic acid bases were fixed in space.

All DFT geometry optimizations were preformed using the NWChem 4.5–4.7 program package [28] on a cluster of dual Intel Itanium2 nodes with Quadrics ELAN4 interconnect. The extensible computational chemistry environment (ECCE) [29,30], which provides a sophisticated graphical user interface and scientific visualization tools, was particularly useful to set up calculations for systems with ‘‘frozen’’ atoms and mixed-basis sets.

2.2. Regular cylindrical projection of electrostatic potential

2.2.1. The idea of regular cylindrical projection

Analysis of electrostatic potential for a molecule is a complicated process. One needs to look at the potential created by charges in the 3D space around the molecule. A simplification is provided by a technique that is called a regular cylindrical projection, which is similar to gnomonic projection methods [31–35]. Here, a fragment of the DNA molecule is positioned at the center of a cylinder and the axis of DNA is aligned with the axis of the cylinder. The shape of a cylinder matches well the structure of a short DNA fragment. The values of EP at the surface of the DNA are projected onto the side wall of the cylinder. It is not necessary to project EP onto the top and bottom of the cylinder because, in the case of DNA, these areas are occupied by other layers of base pairs.

2.2.2. Definition of molecular surface

There is no unique definition of molecular surface because electron density is given by a charge distribution. The molecular surface may be defined in various ways depending on the task. For example, it may be defined by atomic radii [36] or van der Waals radii [37]. In the case of our study, we are interested in a molecular surface that is important for enzymatic recognition. This is the area where the DNA–enzyme interactions take place. The length of a typical hydrogen bond is 1.8–2.2 Å (defined by the distance of atomic centers). On the other hand, electrostatic interaction of charged groups has a long-range character. We believe that an interesting molecular surface might be ca. 1.5–5 Å from centers of the outermost atoms of DNA fragments. In this study, we assumed that the molecular surface is a *solvent-accessible surface* spanned by spheres centered on atomic nuclei with excluded cavities, as they are not accessible to a solvent molecule. The exclusion of cavities not accessible to solvent was done by raining down a probe upon the atoms and stopping the probe just before a collision (van der Waals overlap) would occur. This approach is similar to that presented by Greer and Bush [38]. In our implementation, however, the direction of an approaching probe is perpendicular to the axis of the DNA fragment. We have used a probe with a 1.3 Å radius to simulate a solvent molecule. The radii for the C, N, O, H and P atoms are based on van der Waals radii used in the MM3 force field [39]. The radius for Na is based on its ionic radius. The used radii are presented in Table 1.

The usage of solvent-accessible surface and van der Waals radii is one of the improvements over the previous work [20]. Before, the molecular surface was defined by a union of expanded atom radii, similarly to the approach of Richmod [40]. The expanded radii were derived from covalent radii of atoms increased by an additional radius of a solvent probe of 2 Å. This approach helped to skip the problem of finding a consistent set of van der Waals radii. The current improvement was important to demonstrate that the main features of EP around DNA are insensitive to the details of the accepted DNA surface. This strengthens the chemical importance of our findings presented in Section 3.

Table 1
Values of van der Waals radii for H, N, C, O, P and ionic radius of Na (in Å)

Element	H	C	N	O	P	Na
Radius	1.62[a]	2.04[a]	1.93[a]	1.82[a]	2.22[a]	1.02[b]

[a] Ref. [39].
[b] Ref. [47].

2.2.3. The axis of DNA

In our approach a cylinder is built around the DNA axis. The axis is defined by a point and a vector. For consistency of the EP analysis, they are both kept unchanged when analyzing both the intact and damaged DNA fragments. The point is defined by the geometrical center of the intact DNA fragment. Since our first application of the cylindrical projection to the analysis of EP around DNA [20,21], we have tried a number of ways to calculate the direction vector of the DNA axis (Fig. 2 and Supplementary data, Fig. S-2). We conclude that the most reliable approach it to derive the axis by diagonalization of the tensor of inertia. The eigenvector corresponding to the largest eigenvalue defines the axis of the DNA molecule. This approach works, however, only for molecules with a clearly elongated shape, e.g., the starting DNA dodecamer described in Section 2.1 (Fig. 2, axis a and Supplementary data, Fig. S-1). If it is applied to a shorter DNA fragment, the axis may be even perpendicular to the real axis of the DNA fragment. In case of the 5′-AAC-3′ trimer, the eigenvector corresponding to the largest eigenvalue is 75.55° away from the correct axis (Fig. 2, axis b). It is because the DNA trimer is more box-like (Fig. 2 and Supplementary data, Fig. S-3) and the procedure finds its ''long axis'' (Fig. 2 and Supplementary data, Figs. S-2 and S-3).

In the past we used two other approaches to determine the axis of the DNA molecule. In the first method, the axis is approximated by a vector normal to the top (or bottom) nucleic acid base pair (Supplementary data, Fig. S-4). Since a nucleic acid base pair is not perfectly planar, we approximated the axis of DNA by a vector **z** (Supplementary data, Fig. S-4, bottom) which is a cross-product of vectors connecting atoms N9 and N4 for adenine (vector **b**; Supplementary data, Fig. S-4) and N1 of thymine with N4 of adenine (vector **a**; Supplementary data, Fig. S-4) [41]. Similarly, the **z** vector can be derived from the bottom GC pair. In the second approach we consider line segments between N1 atoms of pyrimidines and N9 atoms of the complementary purine bases. An approximate DNA axis vector bisects these line segments for the top and bottom base pairs (Supplementary data, Fig. S-5). Both approaches provide similar results with the axis differing by, respectively, 7.14 (or 5.57 when the GC pair was used to derive the axis) and 9.77° with respect to the axis labeled ''a'' in Fig. 2, i.e., an eigenvector of the moment of inertia). A graphical representation of the possible DNA axis is presented in Fig. 2 and Supplementary data, Fig. S-2.

2.2.4. Points on the molecular surface

First, we uniformly distribute points on the side wall of the cylinder. It is done in two loops:

(i) Over the height of the cylinder along the z axis (Fig. 3),
(ii) Over the angle α in the xy plane (Fig. 3).

For each step in height (along the z axis), the **R** vector (radius of the cylinder is set to 20 Å) is rotated around the z axis by an angle α and the resulting point on the cylinder is recorded (Supplementary data, Fig. S-6). Each selected point on the cylinder defines a point on the DNA surface (Supplementary data, Fig. S-7). To identify the point on the DNA surface one walks along **R** towards the cylinder axis until one encounters the solvent-accessible DNA surface. This procedure defines a point defined by **R**′ (Fig. 3).

The final electrostatic potential map consists typically of 15,120 points. The angular coordinate was scanned from 0° to 359° with a step of 0.5°. The z coordinate was scanned with 21 steps of 0.5 Å each. The starting point of the z coordinate scan was set to 5.5 Å below the geometrical center of the intact trimer.

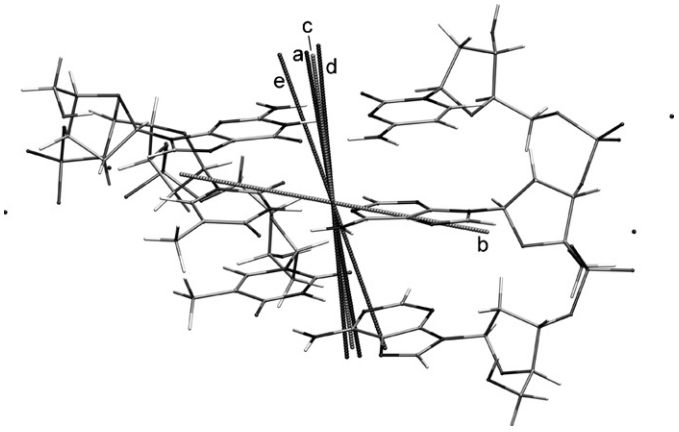

Fig. 2. The cylindrical axis of DNA approximated by different methods: (a) an axis derived from diagonalization of the moment of inertia for the DNA dodecamer (*preferred axis*), (b) an axis derived from diagonalization of the moment of inertia for the DNA trimer, (c) an axis determined by a vector normal to the AT plane, (d) an axis determined by a vector normal to the GC plane and (e) an axis defined by a vector that bisects two line segments between N1 atoms of pyrimidines and N9 atoms of complementary purines (the top and bottom base pairs are considered).

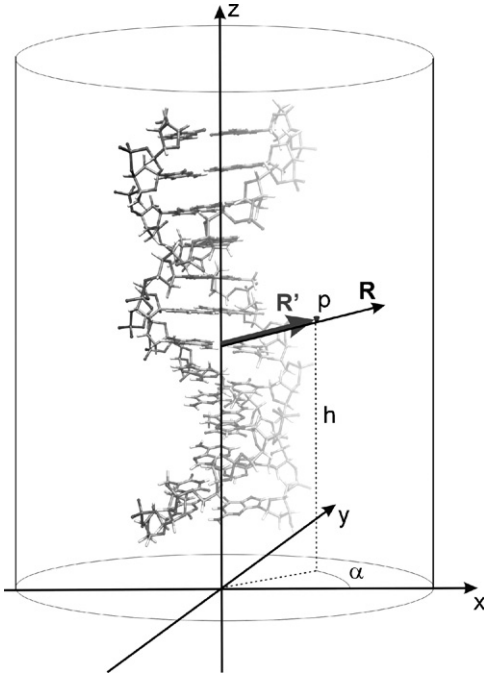

Fig. 3. Details of cylindrical regular projection.

2.2.5. Electrostatic potential on the DNA surface and its 2D map

At each point on the molecular surface, we calculated the EP value directly from the B3LYP/6-31G(d,p) electron density. These calculations were done with the Gaussian03 program [42] on an SGI Altix machine. This type of calculation for large sets of points has become available to us only since recently. Because of limitations on the previously used computers and software, in our previous reports the EP($\vec{p}$) value was calculated as a sum over contributions from all atoms [20,21]:

$$\mathrm{EP}(\vec{p}) = \sum_{n=1}^{N} \frac{q_n}{|\vec{p} - \vec{r}_n|}, \quad (1)$$

where N is the total number of atoms, q_n the charge of the nth atom and $\vec{r}_n$ is the position of the nth atom. The net atomic charges were calculated using the ESP method of Kollman and co-workers [43,44] and default values of atomic radii implemented in the NWChem package [45]. In the ESP method, the charges on atoms are fitted to reproduce the electrostatic potential around the molecule. A detailed comparison of the EP values derived from exact charge density and using the classical Eq. (1) was performed for the intact 5′-AAC-3′ DNA trimer at 3960 points (a map of 360 × 11 points) of the molecular surface. The shape of the EP maps was quite similar for both approaches (the normalized results differed on average by 0.9%). There were, however, some points in which the discrepancies were much larger. Therefore, from here on the values of EP are determined directly from the charge density of DNA fragments. The charge densities are determined in the course of DFT calculations.

The final 2D electrostatic potential maps are presented in Fig. 5 The angle α and the z coordinate of each point are displayed on the horizontal and vertical axis, respectively. The color is assigned according to the value of the electrostatic potential. Red and blue points have positive and negative values of EP, respectively. The maps generated with a smaller number of points (720 × 21) are scaled too a higher resolution (720 × 801) using a bi-directional cubic spline interpolation as implemented in the FreeImage library [46]. The resulting EP maps were analyzed together with the structures of molecules and the accompanying molecular surfaces (Fig. 5 and Supplementary data, Fig. S-7).

3. Results

First, the geometrical differences of the intact and damaged DNA fragments were analyzed. Since both fragments had the same top and bottom nucleic acid base pairs fixed in space during the geometry optimization, it is possible to superimpose those pairs and compare the differences in the remaining molecular parts (Fig. 4 and Supplementary data, Fig. S-8). To clarify the picture, the top and bottom base pairs were removed.

The structural differences between the DNA fragments containing A and 8oxoA are limited to a strand with the lesion. The 8oA is slightly displaced in the direction of the major groove in comparison with the position of A in the intact strand

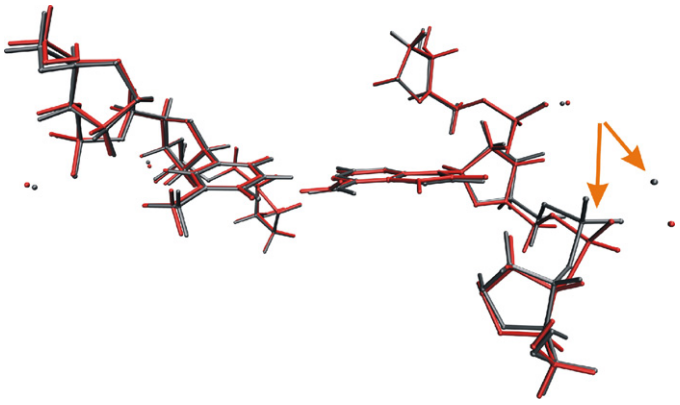

Fig. 4. The superimposed intact (grey) and damaged (red) DNA trimers show differences in geometry. The top and bottom base pairs were removed to clarify the picture. Arrows mark a small relaxation of the damaged strand next to the lesion and a reorganization of sodium countercations.

(Supplementary data, Fig. S-8). Some reorganization of the phosphate group with a sodium countercation next to the lesion might be also observed (Fig. 4). These atoms are moved along the long axis of DNA because of the repulsive interaction between the negatively polarized O8 in 8oA and a negatively charged phosphate group.

The cylindrical projections of EP around the DNA fragments containing A and 8oA show multiple features (Fig. 5 and Supplementary data, Figs. S-9 and S-10). The differences between the EP maps are analyzed in the context of chemical differences between the intact and damaged DNA fragments, which are hidden under the DNA surfaces presented in Supplementary data, Fig. S-7. The most important features are marked on Supplementary data, Figs. S-9 and S-10.

The most distinctive features are sodium countercations that are represented by four big red spots of a positive electrostatic potential (Fig. 5 and Supplementary data, Figs. S-9 and S-10). The sugar-phosphate backbones are represented by two elongated shapes of a neutral potential (Supplementary data, Fig. S-9c). The minor and major grooves might be seen between the two strands (Supplementary data, Fig. S-9b). The grooves are characterized by a negative potential. The contributions from adenine are highlighted in Supplementary data, Fig. S-9e and f. A spot of negative potential associated with N7 (Supplementary data, Fig. S-9f) neighbors a spot of a more neutral potential associated with the N4 amino group (Supplementary data, Fig. S-9e). It must be noted that this feature of the neighboring negative and neutral potentials is very different form the characteristic features of G in 5′-TGT-3′ [21]. In the latter case, there was a big spot of a negative potential resulting from both the N7 and O4 sites of guanine.

At the first glance, the EP map of the DNA fragment with 8oA looks very much like the EP map of the intact fragment (Fig. 5a and b). The sodium countercations, strands, and grooves might be identified in both cases. The intensity of colors, reflecting the values of EP, is very similar except of the middle part of the plot, suggesting that the lesion did not affect much the DNA structure. Features characteristic for 8oA can be identified in the major groove. A spot in the middle of the major

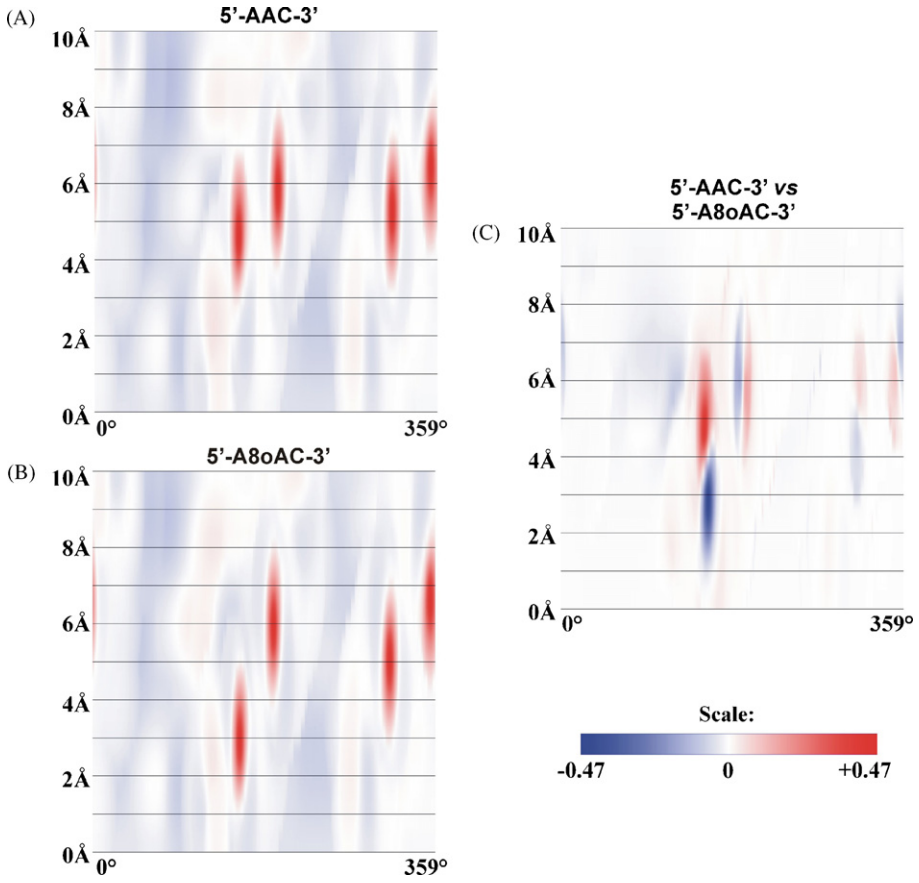

Fig. 5. Electrostatic potential maps of intact (a) and damaged (b) DNA trimers together with a difference map (c). Angular coordinate α is placed on the horizontal axis and the height h is on the vertical axis with zero set to the top AT pair.

groove (Supplementary data, Fig. S-10c), which was related to the N4 amino group in the intact DNA fragment (Supplementary data, Fig. S-9e), becomes broader due to a contribution from the N7 H group in 8oA. Another characteristic feature is associated with O8 of 8oA (Supplementary data, Fig. S-10b). The presence of a negatively charged oxygen atom in 8oA induces a geometrical relaxation of the phosphate backbone, followed by the sodium countercation (see Fig. 4). In consequence of this relaxation, the O8 site is not screened by the phosphate group and becomes clearly recognizable in Supplementary data, Fig. S-10b.

Fig. 5c is a difference map of EP's presented in Fig. 5a and b. It clearly illustrates a significant relocation along the DNA axis of the counteraction that is the nearest to 8oA. Geometrical relaxations of other countercations are also noticeable though less profound. It is remarkable that the geometrical relaxation of countercations has a larger impact on the difference map (Fig. 5c) than those modification that are brought by the protonation of the N7 site and the presence of an additional oxygen in 8oA. The latter modifications are localized in the major groove only and are relatively weak.

4. Summary

We have studied a fragment of intact DNA, 5′-AAC-3′, and its counterpart with A replaced with 8oA (5′-A8oAC-3′) using the B3LYP/6-31G(d,p) method. The geometries of 5′-AAC-3′ and 5′-A8oAC-3′ were optimized with a constraint of the fixed top and bottom base pairs. The electrostatic potential around the DNA fragments was studied using the regular cylindrical projection technique. The values of electrostatic potential at the molecular surfaces were projected onto the side walls of the cylinders surrounding the DNA fragments. The resulting maps of electrostatic potential with accompanying geometries of intact and damaged DNA fragments were analyzed and the results are summarized in the following points:

1. The presence of the 8oA lesion distorts the geometry mainly at the damaged site. The relaxation of the complementary strand is minimal.
2. 8oA is slightly displaced in the direction of the major groove in comparison with the position of A.
3. A reorganization of the phosphate group next to 8oA and the accompanying countercation is an important feature of the 8-oxo-adenine lesion. The relaxation of charged particles along the axis of the DNA fragment is clearly reflected in the electrostatic potential maps.
4. The damaged trimer is characterized by a larger area of a mildly positive electrostatic potential in the major groove than the intact trimer. It is related to the protonation of N7 in 8oA.

5. The damaged trimer is characterized by a larger spot of a negative electrostatic potential in the major groove than the intact trimer. It is related to the presence of O8 in 8oA and the relaxation of the neighboring phosphate and the counter-cation.

We suggest that changes of electrostatic potential around the DNA molecule resulting from chemical modifications of nucleotides may play a role in enzymatic recognition of damaged sites. Our future study will focus on the analysis of the molecular shape of the damaged and undamaged DNA fragments. Molecular dynamics simulations will be preformed to find a correlation between the distribution of countercations and the findings presented here.

Acknowledgements

Helpful discussions Michel Dupuis are gratefully acknowledged. Authors wish to thank Marcel Swart for directing us to a compilation of van der Waals radii. This work was supported by the: (i) US DOE Office of Biological and Environmental Research, Low Dose Radiation Research Program (M.G. and M.H.), (ii) the Office of Science (BER), U.S. Department of Energy, Grant No. DE-FG03-02ER63470 (JHM), (iii) Polish State Committee for Scientific Research (KBN) Grant DS/8221-4-0140-6 (MG), (iv) European Social Funds (EFS) ZPORR/2.22/II/2.6/ARP/U/2/05 (M.H.). M.H. holds the Foundation for Polish Science (FNP) award for young scientists. The calculations were performed at the Academic Computer Center in Gdańsk (TASK) and at the Molecular Science Computing Facility (MSCF) in the William R. Wiley Environmental Molecular Sciences Laboratory, a national scientific user facility sponsored by the U.S. Department of Energy's Office of Biological and Environmental Research and located at the Pacific Northwest National Laboratory, which is operated by Battelle for the U.S. Department of Energy. The MSCF resources were available through a pilot project.

Appendix A. Supplementary data

Supplementary data associated with this article can be found, in the online version, at: doi:10.1016/j.jmgm.2006.12.005.

References

[1] M. Dizdaroglu, P. Jaruga, M. Birincioglu, H. Rodriguez, Free radical-induced damage to DNA: mechanisms and measurements, Free Radic. Biol. Med. 32 (2002) 1102–1115.
[2] W.K. Lutz, Endogenous genotoxic agents and processes as a basis of spontaneous carcinogenesis, Mutat. Res. 238 (1990) 287–295.
[3] B.N. Ames, Endogenous DNA damage as related to cancer and aging, Mutat. Res. 214 (1989) 41–46.
[4] B.N. Ames, Mutagenesis and carcinogenesis: endogenous and exogenous factors, Env. Mol. Mutagen. 14 (1989) 66–77.
[5] B.N. Ames, L.S. Gold, Endogenous mutagens and the causes of aging and cancer, Mutat. Res. 250 (1991) 3–16.
[6] P. Jaloszynski, P. Jaruga, R. Olinski, W. Biczysko, W. Szyfter, E. Nagy, L. Moller, K. Szyfter, Oxidative DNA base modifications and polycyclic aromatic hydrocarbon DNA adducts in squamous cell carcinoma of larynx, Free Radic. Res. 37 (2003) 231–240.
[7] C. Von Sonntag, The Chemical Basis of Radiation Biology, Taylor and Francis, New York, 1987.
[8] (a) M. Dizdaroglu, Oxidative damage to DNA in mammalian chromatin, Mutat. Res. 275 (1992) 331–342;
(b) A.P. Breen, J.A. Murphy, Reactions of oxyl radicals with DNA, Free Radic. Biol. Med. 18 (1995) 1033–1077;
(c) M. Dizdaroglu, Mechanisms of free radical damage to DNA, in: O.I. Aruoma, B. Halliwell (Eds.), DNA and Free Radicals: Techniques, Mechanisms and Applications, OICA International, St. Lucia, 1998 , pp. 3–26.
[9] T. Lindahl, Instability and decay of the primary structure of DNA, Nature 362 (1994) 709–714.
[10] J.C. Fromme, A. Banerjee, S.J. Huang, G.L. Verdine, Structural basis for removal of adenine mispaired with 8-oxoguanine by MutY adenine DNA glycosylase, Nature 427 (2004) 652–656.
[11] Y.J. Wang, Y.S. Ho, M.J. Lo, J.K. Lin, Oxidative modification of DNA bases in rat liver and lung during chemical carcinogenesis and aging, Chem. Biol. Interact. 94 (1995) 135–145.
[12] P. Jaruga, M. Dizdaroglu, Repair of products of oxidative DNA base damage in human cells, Nucleic Acids Res. 24 (1996) 1389–1394.
[13] H. Kamiya, N. Murata-Kamiya, S. Koizume, H. Inoue, S. Nishimura, E. Ohtsuka, 8-Hydroxyguanine (7,8-dihydro-8-oxoguanine) in hot spots of the c-Ha-ras gene: effects of sequence contexts on mutation spectra, Carcinogenesis 16 (1995) 883–889.
[14] H. Kamiya, H. Miura, N. Murata-Kamiya, H. Ishikawa, T. Sakaguchi, H. Inoue, T. Sasaki, C. Masutani, F. Hanaoka, S. Nishimura, E. Ortsuka, 8-Hydroxyadenine (7,8-dihydro-8-oxoadenine) induces misincorporation in in vitro DNA synthesis and mutations in NIH 3T3 cells, Nucleic Acids Res. 23 (1995) 2893–2899.
[15] E.C. Friedberg, G.C. Walker, W. Siede, DNA Repair and Mutagenesis, ASM Press, Washington, DC, 1995.
[16] S.S. Wallace, Enzymatic processing of radiation-induced free radical damage in DNA, Radiat. Res. 150 (1998) S60–S79.
[17] A.S. Bernards, J.K. Miller, K.K. Bao, I. Wong, Flipping duplex DNA inside out, J. Biol. Chem. 277 (2002) 20960–20964.
[18] G. Slupphaug, C.D. Mol, B. Kavli, A.S. Arvai, H.E. Krokan, J.A. Tainer, A nucleotide-flipping mechanism from the structure of human uracil—DNA glycosylase bound to DNA, Nature 384 (1996) 87–92.
[19] M. Bjoras, E. Seeberg, L. Luna, L.H. Pearl, T.E. Barrett, Reciprocal "flipping" underlies substrate recognition and catalytic activation by the human 8-oxo-guanine DNA glycosylase, J. Mol. Biol. 317 (2002) 171–177.
[20] M. Haranczyk, R.A. Bachorz, I. Dabkowska, M. Dupuis, J.H. Miller, M.S. Gutowski, Computational characterization of lesions in DNA, in: 228th ACS National Meeting, U175-U175, 025-BIOL Part 1, Philadelphia, PA, August 22–26, 2004.
[21] M. Harańczyk, M. Gutowski, Differences in electrostatic potential around DNA fragments containing guanine and 8-oxo-guanine, Theoretical Chemistry Accounts, DOI:10.1007/s00214-006-0133-1.
[22] J.H. Miller, A. Aceves-Gaona, M.B. Ernst, M. Haranczyk, M. Gutowski, E.R. Vorpagel, M. Dupuis, Structure and energetics of clustered damage sites, Radiat. Res. 164 (2005) 582–585.
[23] S. Arnott, D.W.L. Hukins, Optimised parameters for A-DNA and B-DNA, Biochem. Biophys. Res. Commun. 47 (1972) 1504–1509.
[24] A.D. Becke, Density-functional exchange–energy approximation with correct asymptotic behavior, Phys. Rev. A 38 (1988) 3098–3100.
[25] A.D. Becke, Density-functional thermochemistry. III. The role of exact exchange, J. Chem. Phys. 98 (1993) 5648–5652.
[26] C. Lee, W. Yang, R.G. Paar, Development of the Colle–Salvetti correlation–energy formula into a functional of the electron density, Phys. Rev. B 37 (1988) 785–789.
[27] W. Kohn, Y. Meir, D.E. Makarov, van der Waals energies in density functional theory, Phys. Rev. Lett. 80 (1998) 4153–4156.
[28] (a) T.P. Straatsma, E. Apra, T.L. Windus, E.J. Bylaska, W. de Jong, S. Hirata, M. Valiev, M. Hackler, L. Pollack, R. Harrison, M. Dupuis, D.M.A. Smith, J. Nieplocha, V. Tipparaju, M. Krishnan, A.A. Auer, E. Brown, G. Cisneros, G. Fann, H. Früchtl, J. Garza, K. Hirao, R. Kendall, J. Nichols, K. Tsemekhman, K. Wolinski, J. Anchell, D. Bernholdt, P. Borowski, T.

Clark, D. Clerc, H. Dachsel, M. Deegan, K. Dyall, D. Elwood, E. Glendening, M. Gutowski, A. Hess, J. Jaffe, B. Johnson, J. Ju, R. Kobayashi, R. Kutteh, Z. Lin, R. Littlefield, X. Long, B. Meng, T. Nakajima, S. Niu, M. Rosing, G. Sandrone, M. Stave, H. Taylor, G. Thomas, J. van Lenthe, A. Wong, Z. Zhang, NWChem, A Computational Chemistry Package for Parallel Computers, Version 4, Pacific Northwest National Laboratory, Richland, WA 99352-0999, USA, 2004;
(b) R.A. Kendall, E. Aprà, D.E. Bernholdt, E.J. Bylaska, M. Dupuis, G.I. Fann, R.J. Harrison, J. Ju, J.A. Nichols, J. Nieplocha, T.P. Straatsma, T.L. Windus, A.T. Wong, High performance computational chemistry: an overview of NWChem a distributed parallel application, Comput. Phys. Commun. 128 (2000) 260–283.

[29] G. Black, B. Didier, T. Elsethagen, D. Feller, D. Gracio, M. Hackler, S. Havre, D. Jones, E. Jurrus, T. Keller, C. Lansing, S. Matsumoto, B. Palmer, M. Peterson, K. Schuchardt, E. Stephan, L. Sun, H. Taylor, G. Thomas, E. Vorpagel, T. Windus, C. Winters, Ecce, A Problem Solving Environment for Computational Chemistry, Software Version 3.2.5, Pacific Northwest National Laboratory, Richland, WA 99352-0999, USA, 2006.

[30] G.D. Black, K.L. Schuchardt, D.K. Gracio, B. Palmer, The extensible computational chemistry environment: a problem solving environment for high performance theoretical chemistry, in: P.M.A. Sloot, D. Abramson, A.V. Bogdanov, J. Dongarra (Eds.), Computational Science—ICCS 2003, International Conference Proceedings 2660, vol. 81, Saint Petersburg, Russian Federation, Melbourne, Australia, Springer Verlag, Berlin, Germany, 2003, pp. 122–131.

[31] V.J. van Geerestein, N.C. Perry, P.G. Grootenhuis, C.A.G. Haasnoot, 3D Database searching on the basis of ligand shape using the SPERM prototype method, Tetrahedron Comput. Methodol. 3 (1990) 595–613.

[32] N.C. Perry, V.J. van Geerestein, Database searching on the basis of three-dimensional molecular similarity using the SPERM program, J. Chem. Inf. Comp. Sci. 32 (1992) 607–616.

[33] P.-L. Chau, P.M. Dean, Molecular recognition: 3D surface structure comparison by gnomonic projection, J. Mol. Graph. 5 (1987) 97–100.

[34] F.E. Blaney, C. Edge, R.W. Phippen, Molecular surface comparison. 2. Similarity of electrostatic vector fields in drug design, J. Mol. Graph. 13 (1995) 165–174.

[35] A.R. Leach, V.J. Villet, An Introduction to Chemoinformatics, Kluwer Academic Publishers, 2003,, p. 118.

[36] A.F. Wells, Structural Inorganic Chemistry 5/E (Polish Translation), Wydawnictwa Naukowo-Techniczne, Warszawa, 1993, p. 256.

[37] A. Bondi, van der Waals volumes and radii, J. Phys. Chem. 68 (1964) 441–451.

[38] J. Greer, B. Bush, Macromolecular shape and surface maps by solvent exclusion, Proc. Natl. Acad. Sci. U.S.A. 75 (1978) 303–307.

[39] N.L. Allinger, X. Zhou, J. Bergsma, Molecular mechanics parameters, J. Mol. Struct. (Theochem.) 312 (1994) 69–83.

[40] T.J. Richmod, Solvent-accessible surface area and excluded volume in proteins. Analitical equations for overlapping spheres and implications for the hydrophobic effect, J. Mol. Biol. 178 (1984) 63–89.

[41] In the previous implementation of the cylindrical projection, this approximate axis of the DNA fragment goes through a point in the middle of the line connecting N1 of thymine with N9 of adenine.

[42] M.J. Frisch, G.W. Trucks, H.B. Schlegel, G.E. Scuseria, M.A. Robb, J.R. Cheeseman, J.A. Montgomery Jr., T. Vreven, K.N. Kudin, J.C. Burant, J.M. Millam, S.S. Iyengar, J. Tomasi, V. Barone, B. Mennucci, M. Cossi, G. Scalmani, N. Rega, G.A. Petersson, H. Nakatsuji, M. Hada, M. Ehara, K. Toyota, R. Fukuda, J. Hasegawa, M. Ishida, T. Nakajima, Y. Honda, O. Kitao, H. Nakai, M. Klene, X. Li, J.E. Knox, H.P. Hratchian, J.B. Cross, V. Bakken, C. Adamo, J. Jaramillo, R. Gomperts, R.E. Stratmann, O. Yazyev, A.J. Austin, R. Cammi, C. Pomelli, J.W. Ochterski, P.Y. Ayala, K. Morokuma, G.A. Voth, P. Salvador, J.J. Dannenberg, V.G. Zakrzewski, S. Dapprich, A.D. Daniels, M.C. Strain, O. Farkas, D.K. Malick, A.D. Rabuck, K. Raghavachari, J.B. Foresman, J.V. Ortiz, Q. Cui, A.G. Baboul, S. Clifford, J. Cioslowski, B.B. Stefanov, G. Liu, A. Liashenko, P. Piskorz, I. Komaromi, R.L. Martin, D.J. Fox, T. Keith, M.A. Al-Laham, C.Y. Peng, A. Nanayakkara, M. Challacombe, P.M.W. Gill, B. Johnson, W. Chen, M.W. Wong, C. Gonzalez, J.A. Pople, Gaussian 03, Revision C.02, Gaussian Inc., Wallingford, CT, 2004.

[43] B.H. Besler, K.M. Merz Jr., P.A. Kollman, Atomic charges derived from semiempirical methods, J. Comp. Chem. 11 (1990) 431–439.

[44] U.C. Singh, P.A. Kollman, An approach to computing electrostatic charges for molecule, J. Comp. Chem. 5 (1984) 129–145.

[45] Atomic radii used for ESP calculation (Merz–Kollman scheme): H, 1 Å, C, 1.47 Å, N, 1.4 Å, O, 1.36 Å, Na, 2.1 Å and P, 1.8 Å.

[46] http://freeimage.sourceforge.net.

[47] D.F. Shriver, P.W. Atkins, C.H. Langford, Inorganic Chemistry, second ed., Oxford University Press, 1995,, p. 35.